International Nano Letters (2021) 11:307–319
https://doi.org/10.1007/s40089-021-00343-z

REVIEW

Review on structural and magnetic properties of (Co–Zn) ferrite nanoparticles

R. Sagayaraj[1] · S. Aravazhi[2] · G. Chandrasekaran[3]

Received: 23 December 2020 / Accepted: 17 May 2021 / Published online: 2 June 2021

Abstract
Mixed spinel ferrites are very popular because of their excellent flexible magnetic and electronic properties. This systematic review followed the guidelines for repotting physicochemical properties of Co–Zn ferrite. Non-magnetic cations doped (Zn^{2+}) cobalt ferrite to tune the structural and magnetic properties of the mixed spinel ferrite. In this review, paper focuses on various synthesis methods, change of pH, change of sintering, change of dopant and change of surfactant summarized for real-time applications.

Keywords Nanoferrite · Nanomaterials · Nanoproperties · Nanoparticles · Nanospinel ferrites

Introduction

Ferrites are materials of ferromagnetic oxide that have high resistivity and permeability. While ferrite magnetization is less than half the saturation of ferromagnetic alloys, it has advantages such as higher frequency applicability, high resistivity, lower price, higher heat and higher resistance to corrosion. The spinel ferrites have excellent potential applications in many fields, such as anti-cancer drugs, active components of ferrofluids, antennae, antenna rods, biomedical sensors, biomedicine electronics, catalysis, catalytic insulators, coatings, cellular therapy, electronic circuits power delivering devices, electromagnetic interference suppression, filters circuit, computer, colour imaging, cellular phones, drug delivery, digital diaries, disk recording, detoxification of biological fluids, ferrofluids, flexible recording media, gas detectors, information and energy storage media, instance microwave ovens, magnetic refrigeration, magnetic refrigeration, magnetic drug delivery, memory storage devices, mechanical hardness, magnetic resonance imaging (MRI) contrast enhancement, magnetic recording media, medical devices, magnetic sensors, magnetic cell separation, magnetic devices, magnetic anisotropy, microwave fascinating materials, magnetic soundtrack, microwave devices, magneto-optical recording media, switching devices, transformer cores, high-frequency systems, hyperthermia treatment, high-density digital recording disc, high-frequency transformers, satellite communication, solar energy conversion, sensors, satellite dish rod, magnetic fluid, permanent magnets, photo catalysis, hard disc recording media, radar devices, recording tapes, recording heads, recorder, read–write heads, high-frequency electric devices, video tape, video camera, transformer cores, tissue repair, TV, permanent magnets, loading coils, local communication [1–5]. Magnetism was observed as early as 800 BC in a naturally occurring material called load stone (Fe_3O_4) which was used for navigation purposes. Ferrites are very famous magnetic materials. Ferrites are dark grey and black. Ferrites are insulator materials possessing both electrical and magnetic attributes. Ferrites have less value of dielectric loss. Ferrites have a high value of permeability, constant magnetization in M–H curve and electrical resistivity [6]. In materials such as Fe, Ni, Co and Mn, let us describe the roots of magnetism. Let us begin with the simple fact that atoms create materials. Each atom contains an electron(s). Most people know that they have charging electrons. What people have not understood for many years (a century ago) is that electrons also have a spin-like property. There might

✉ R. Sagayaraj
sagayarajnancy@gmail.com

[1] PG& Research Department of Physics, St. Joseph's College of Arts and Science (Autonomous), Cuddalore, Tamilnadu 607001, India

[2] Department of Physics, Arignar Anna Arts College, Villupuram, Tamilnadu 605602, India

[3] Department of Physics, Pondicherry University, Pondicherry 605014, India

be an up or down spin on an electron. Let me say, to make things less confusing, that the electron is a tiny magnet. We can picture a spin-up electron with its north pole up as a magnet, and the spin-down electron has its south pole up. Besides spin, an electron's orbital motion around the nucleus (sort of like the planet moving around the sun) also creates a magnetic field, but in most materials it is not important and we can disregard it. We now realize, roughly, that every electron is a small magnet. The atoms would not behave like a magnet if an atom had an equal amount of electrons spinning up and down. In certain materials, such as iron, nickel, cobalt, and manganese, there is an unequal sum of spin-up and spin-down electrons. It is possible to think of those atoms as magnets. Please note that out of several elements that can be thought of as magnets, only a few of the elements have atoms. Now, let us move on to a larger view, where we bring together some atoms. "If, somehow, all atoms may have the same orientation (say, the north poles of all the magnets pointing in the same direction), because of" exchange interaction, "a finding from quantum mechanics, the substance can behave like a magnet. The magnetic properties of atoms are cancelled without exchange interactions and the substance is not magnetic. To sum up, there are only a few elements that have an unequal number of electrons spin-up and spin-down, which also have an association of exchange that holds them in the same direction. Such components are magnetic. The aim was to explore variations in the structural and magnetic performance of cobalt ferrite powders with partial non-magnetic zinc cation substitution.

Primary results

Diamagnetic materials, paramagnetic materials (PM), ferromagnetic materials (FM), antiferromagnetic materials (AFM), super paramagnetic materials (SPM) and ferrimagnetic materials (Ferrites) are classified through magnetic materials.

Diamagnetic materials

M–H loops of diamagnetic samples as shown in Fig. 1. Diamagnetism is a very weak effect and is observed in solids, which do not contain any permanent magnetic moments. The presence of a tiny non-zero magnetic moment exists. For diamagnetic compounds, the magnetic sensitivity is negative and relative permeability is marginally less than unity.

It is very weak in resistance to solids, so it can only be detected when other forms of magnetism are totally absent. Diamagnetism will only be detected where all forms of magnetism are entirely absent. For ionic and covalent crystals, diamagnetism is observed. On the

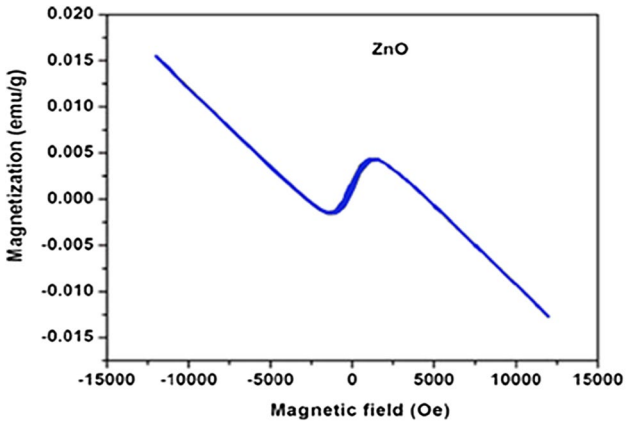

Fig. 1 M–H loops of diamagnetic samples (reproduced from Ref. [7] with permission from Journal of Luminescence)

principle of electronegativity, the theory of the state of oxidation clearly functions. The most electronegative the atom has the negative charge, and the less electronegative the atom has the positive charge. Zinc's most common oxidation number is +2 (Zn^{2+}). And the oxidation level of oxygen is -2 (O^{2-}). In chemicals, there may also be an oxidation state, not just elemental oxygen. There is zinc oxide known. In the oxidation state formalism, this molecule with the structural formula Zn–O–O–Zn has oxygen receiving an electron from zinc but losing one to Zn. Diamagnetic (non-magnetic) means entirely coupled orbital's, i.e. They have a paired electron and no electron that is unpaired. Similarly, Zn^{2+} looses two electrons from the orbital 4 s, so you can get 3d orbital completely filled and no unpaired electrons again. Zn and Zn^{2+} are thus, diamagnetic [6, 8].

Paramagnetic materials

Figure 2 shows the M–H loops of paramagnetic materials observed using VSM. Paramagnetic material occurs because, due to insufficient cancellation of electron spin and/or orbital magnetic moments, the compounds keep a lasting dipole moment. Without a magnetic field, these magnetic dipole moments are guided consistently, bringing about no net magnetization.

The paramagnetic is sensitive to the temperature, the lower the temperature, the stronger the effect. There is more alignment at low temperature when the effect of thermal motion is less. Paramagnetism occurs in atom and ions having odd number of electrons since they possess angular momentum and, therefore, must be paramagnetic. Transition group ions with incomplete 3d, 4d, 5d, 4f or 5f shell show paramagnetic. Ions with ionic radii (Table 1) are Fe^{3+},Fe^{2+},Co^{2+},Ni^{2+},Cu^{2+},Zn^{2+} etc. [6, 10].

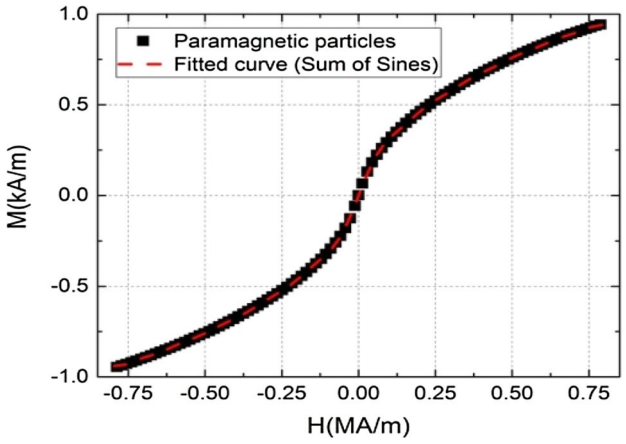

Fig. 2 M–H loops of paramagnetic particles (reproduced from Ref. [9] with permission from IEEE Access)

Table 1 Various ionic radii

Cations	Ionic radius (Å)
Fe^{2+}	0.77 [3]
Fe^{3+}	0.60 [1]
Zn^{2+}	0.82 [11]
Co^{2+}	0.75 [12]

Ferromagnetic materials

Figure 3 shows the various magnetic materials specified in an applied field. Even in the absence of a magnetic field, the magnetic material experiences a parallel alignment of the torque resulting in a large magnetization. Atomic moments in these supplies show very stable interactions with paramagnetic materials. The parallel or antiparallel coordination of atomic moments results for interactions involving the exchange force of ions. Ferromagnetism is shown by the Fe, Ni and Co elements and by many of their alloys. This means that it applies to 3d and 4f partly filled shells. Spontaneous magnetization and magnetic temperature control known as Curie temperature control are two distinct features of ferromagnetic materials such as multi-domain properties and single-domain properties (Table 2).

The ferromagnetic activity of the material is destroyed above the Curie temperature as a randomizing effect, caused by thermal energy, is more prominent above that temperature than the electronic exchange forces [6].

Antiferromagnetic materials

In antiferromagnetic materials coupling between adjacent atoms or ions causes an antiparallel alignment, resulting in the vanishing of magnetic moment over a finite volume. Case of manganese oxide (MnO) shows antiferromagnetic activity (Fig. 3). MnO is an ion complex of both Mn^{2+} and

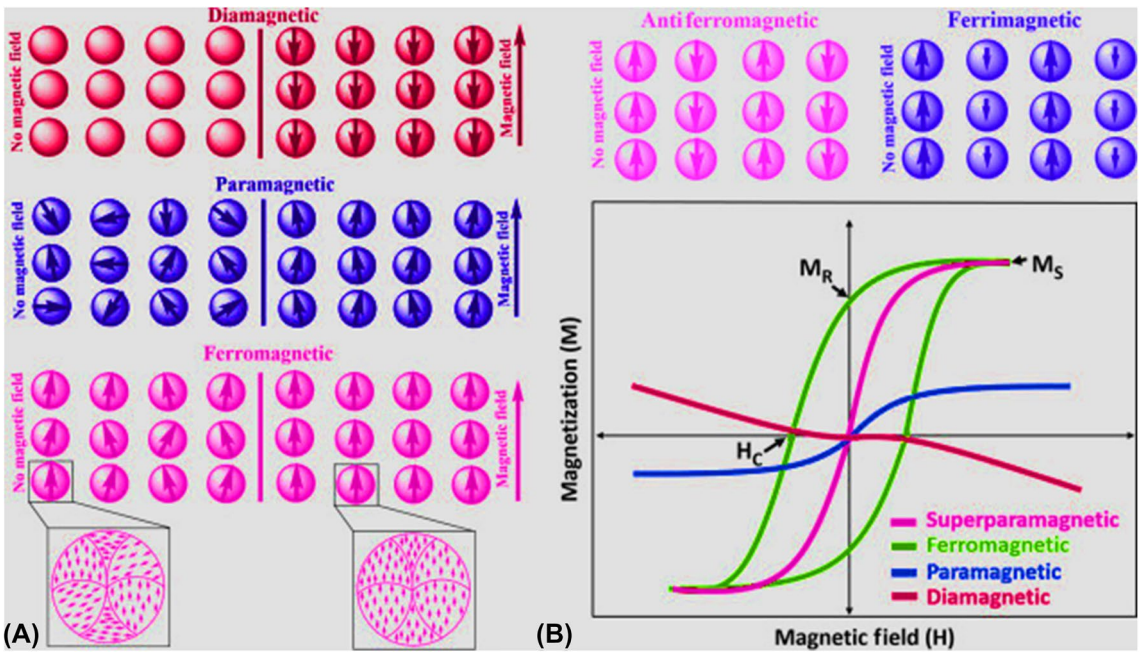

Fig. 3 **A** Various types of magnetic materials (diamagnetic, paramagnetic, ferromagnetic, antiferromagnetic, and ferrimagnetic), **B** representative hysteresis loops that illustrate the magnetic behavior of materials when an external field is applied (reproduced from Ref [13] with permission from Smart Nanoparticles for Biomedicine)

Table 2 Materials properties

Property	Ferromagnetism	Superparamagnetism
Structure	Multiple domains[2, 14]	Single-domain particle [15–18]
Magnetic memory	Yes[2, 14]	None
Degree of induced magnetization	Very high[2, 14]	Moderate[19–21]

O^{2-} ions. Since spin and orbital magnetic moments are absolutely cancelled, no net magnetic moment is correlated with O2-ions. The Mn^{2+} ions, which are primarily due to spinning magnetic moments, have a net magnetic moment. The Mn^{2+} ions coordinate unique moments like those in the crystal structure. They are antiparallel to opposite ions and thus have no net magnetic moment. Due to the antiferromagnetic ordering of Fe^{3+} ions in the B-sites, $ZnFe_2O_4$ is a standard spinel where A-sites and bulk are dominated by non-magnetic Zn ions, $ZnFe_2O_4$ is non-magnetic, nanometer-scale inversion rises, and all A-sites and B-sites are occupied by non-magnetic Zn ions. This adds to the conventional rule that the non-magnetic $ZnFe_2O_4$ is broken down and magnetized. Over a critical temperature referred to as the temperature of Neel, the character of antiferromagnetism should vanish [6, 15, 22].

Similarly, cobalt ferrite doped with zinc or zinc ferrite doped with cobalt doped with zinc in which the antiferromagnetic character was sufficiently active and coercivity and magnetization in the products decreased. Various kinds of ordering of magnetic ions as seen in Fig. 3A. The cations need, which can be obstructed by grain growth (ionic radius), are not entirely fulfilled for synthesized materials (antiferromagnetic).The greater bond energy of $Co^{2+}\leftrightarrow O^{2-}$leads to a reduction in the particle sizes of the samples as compared to $Zn^{2+}\leftrightarrow O^{2}$as the zinc content increases with resulting decreases in coercivity. However, the average crystalline size is continuously influenced by the rise in Zn ions, which is related to the pH value. Therefore, it determines the relationship between the magnetic order and the distribution of cations. As the chemical environment differs from that of the oxygen-coordinated core atoms, this is further supported by its distinct isomer shift [2, 15, 19, 23].

Super paramagnetic material

Variation of magnetic signature due to particle size as shown in Fig. 4. Superparamagnetic is a special magnetism behavior that occurs between ferromagnetic properties and ferromagnetic properties. Under the control of temperature in relatively small nanoparticles, the magnetization will spontaneously change direction. A standard time is called the Neel relaxation time between two flips.

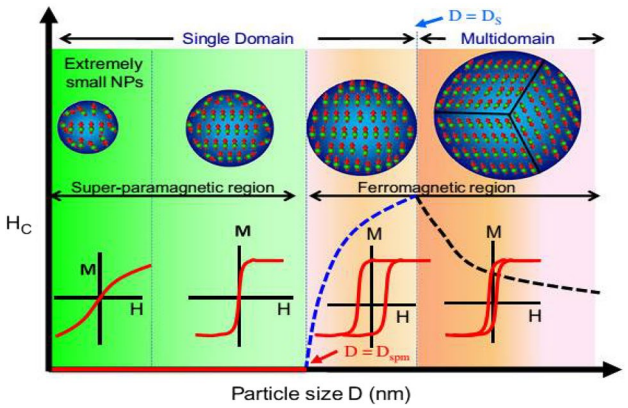

Fig. 4 Variation of magnetic signature due to particle size (reproduced from Ref. [24] with permission from Handbook of Magnetic Materials)

When, without an outside magnetic field, the time used to compute the magnetization of nanoparticles is any longer than the time of Neel relaxation, their normal magnetization esteemed will in general be zero: they are supposed to be in a super paramagnetic condition. In this condition, like a paramagnet, an outside magnetic field can magnetize the nanoparticles. In any case, their magnetic affectability is a lot more significant than that of the paramagnets. Any ferromagnetic or ferrimagnetic material ordinarily goes through progress to a paramagnetic state over its Curie temperature. Since it happens underneath the Curie temperature of the material, superparamagnetism is unmistakable from this common change. In single-domain nanoparticles, i.e., containing a single magnetic domain, superparamagnetic occurs. This is conceivable when their measurement is under 3–50 nm, contingent upon the materials. Here, the magnetization of the nanoparticles, the amount of the multitude of individual magnetic moments conveyed by the nanoparticle atoms, is known as a single giant magnetic moment [6, 25–27].

Ferrimagnetic materials

The neighboring magnetic moments align themselves antiparallel to each other in ferrimagnetisms (Fig. 3), but their magnitude is not the same, so there is a net magnetic moment. Garnets, ferrite, etc. are examples of ferrimagnetic materials. Ferrimagnetic materials exhibit spontaneous magnetization, remanence and other features close to ordinary ferromagnetic materials; however, the spontaneous moment may not conform to the predicted value of the dipoles in complete parallel alignment. Ferrites are known to have a collinear ferrimagnetic composition, according to Neel's model, in which the magnetization of the sublattice tetrahedral is antiparallel to that of the sublattice octahedral

(B). The A-sublattice/sites and the magnetic moment of the B-sublattice/sites balance each other out of this way. Net material magnetization is due to B-sublattice/void magnetization, since B-sublattice/void magnetization is greater than A-sublattice magnetization. Therefore, the sample offers a high saturation induction value Compared to 'A'–'A' interaction, the interaction between magnetic ions of sublattices 'A' and 'B' (A–B interaction) is the strongest, almost ten times weaker, followed by the weakest 'B'–'B'. The prevailing relationship between 'A' and 'B' leads to full or partial ferrimagnetisms (non-compensated) [6, 11, 14, 28].

Soft ferrites

Magnetic moments displayed in Fig. 5 on the hard/soft interface of exchange-coupled ions. Soft ferrite is an electromagnetic ceramic material with very strong and brittle properties, dark grey or black. Soft ferrites have little to do with their physical properties, but are related to their magnetic properties. Soft ferrites have not preserved a significant magnetization, although magnetization is known to be permanent in hard ferrites. Soft ferrite is the common term for the grouping of ceramic and electromagnetic materials. Soft ferrites from the crystallographic aspect are inverse spinals and belong to the cubic crystal structure. In other words, soft ferrites display a homogeneous cubic spinel crystalline structure and consist of iron oxide with divalent metal oxides. Magnetic domain theory means that these interactions create magnetic domains that are microscopic magnetized areas within the material. Although local domains are fully magnetized where there is no magnetizing power, the magnetic domains are random and the net flux contribution is zero.

When a magnetizing force is present, the magnetic domains converge toward of the magnetizing force, resulting in a significant net flux contribution. Soft ferrite is also

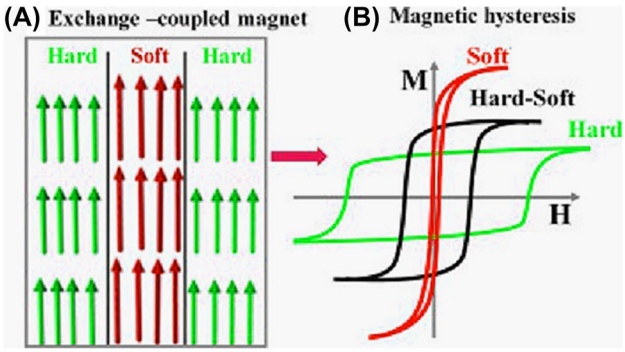

Fig. 5 **A** Magnetic moments at the hard/soft interfaces of an exchange-coupled ion, **B** The corresponding magnetic hysteresis curves (reproduced from Ref. [24] with permission from Handbook of Magnetic Materials)

a semiconductor in which coercivity, retentivity and low loss of hysteresis, it can induce electron flow through the material anywhere between conductors and insulators [29]. The coercive field (Hc) relies strongly on the magnetic field required to pass the magnetic anisotropy barrier, according to the theory of Stoner–Wolfforth (S–W). As the productive magnetic anisotropy decreases (or increases), the external magnetic field required for spin reversal often decreases (or increases).This is one of the possible explanations in coercive fields for the variance. The other possible element that alters coercivity is magnetization of saturation (Ms). Indeed, coercivity is primarily associated with shifts in the magnetization values of saturation. Hc increases as the effective magnetic anisotropy increases, according to the S–W principle. However, if Ms Increases, the value of Hc decreases. In the present analysis, the effective magnetic anisotropy increases within the ferrite system due to the reduction of thermal variations at lower temperatures. This theory also tends to distinguish coercivity and saturation magnetization as hard and soft ferrite [15, 19, 30].

Hard ferrites

Even after the removal of the applied magnetizing field, heavy magnetization persists with hard ferrites, and residual magnetization is stable even if certain strength of the demagnetizing field is applied. Broad classes of ceramic materials are formed by these ferrites. Hard ferrites are often very hard and brittle and vary in colour from dark grey to black. Hard ferrite is weak and naturally occurring magnetite. Hard ferrite is an irreversible magnetism properties which is possessed naturally. Permanent magnetic hard ferrites play a dominant position, primarily due to the low price per unit of available energy, Strong chemical quality and high raw materials availability. It is possible to accept M type ferrites as the more common form of hard ferrites. Interstitial positions are surrounded by a magnetoplumbite structure characterized by a tight packing of Fe atom oxygen and metal ions. Alternatively, this crystal structure can be represented as cubic blocks with a spinal structure and hexagonal blocks containing metal ions [16, 31, 32].

Discussions

Zinc doped with cobalt ferrite ($Co_{1-x}Zn_xFe_2O_4$) synthesized by a low-cost co-precipitation technique [2]. Calcinations temperature (C_T) and potential hydrogen (pH) have been set at 800 °C and 11, respectively (Table 3). As Zn increases, the lattice parameter varies from 8.33–8.35 Å and its crystallite size varies from 28 to 31 nm. The magnetization varied from 0.31 emu/g to 0.75 emu/g. The $Co_{1-x}Zn_xFe_2O_4$ spinel ferrite device was prepared using the sol–gel auto-combustion

Table 3 Co–Zn ferrite nature and its specifications

Compound and method	Structure	D (nm)	a (Å)	FST	MST	M_S emu/g	Hc Oe	C_T (°C)		S	R
$Co_{1-x}Zn_xFe_2O_4$ Co-precipitation	Cubic	28–31	8.33–8.35	Normal spinel	Ferromagnetic	0.31–0.75	1678.6–270.20	800	11	PVP	[2]
$Co_{1-x}Zn_xFe_2O_4$ sol–gel auto-combustion	Cubic	45–49	8.38–8.43	Normal spinel	Ferrimagnetic	65.628–5.316	1116.9–113.48	600	7	Citric acid	[14]
$Co_{0.5}Zn_{0.5}Fe_2O_4$ sol–gel	Cubic	13				–	–	400	10.5	PVA	[33]
$Co_{1-x}Zn_xFe_2O_4$ sol–gel auto-combustion	Cubic	18.99–41.49	8.38–8.41	Mixed spinel	Ferrimagnetism	21.38–65.68	9.56–79.9	800		Starch	[23]
$Co_{1-x}Zn_xFe_2O_4$ sol–gel	–	11–28	8.47 -8.52	Mixed spinel	Ferrimagnetism	60.92–74.67	2000–170	400	–	–	[12]
$Zn_{1-x}Co_xFe_2O_4$ facile reduction−oxidation route	–	9–27	8.42–8.34	Mixed spinel	Ferrimagnetism	4–51	32	120	–	–	[11]
$Co_{1-x}Zn_xFe_2O_4$ co-precipitation	Cubic	27–55	8.35–8.40	Mixed spinel	Ferromagnetic	91–114	75–1382	800	–	–	[34]
$Co_{0.6}Zn_{0.4}Fe_2O_4$ hydrothermal	–	90		inverse spinel	Superparamagnetism	55	35	160	11	–	[10]
$Zn_xCo_{1-x}Fe_2O_4$ hydrothermal co-precipitation	Cubic	8–10	–	Mixed spinel	Super para	–	215–630	300	–	–	[8]
$Co_{1-x}Zn_xFe_2O_4$ Auto-combustion	Cubic	34–45	8.37—8.44	–	–	–	–	900		Citric acid	[16]
$Co_{1-x}Zn_xFe_2O_4$ auto-combustion	Cubic	20–58	8.37–8.42	Mixed spinel	Ferromagnetic	8.5–67.6	265–1265	–	7	sucrose	[35]
$CoFe_{2-x}Zn_xO_4$ microwave gel combustion	Cubic	12–15	8.35- 8.58	mixed spinel	–	73–129	183–890	600	-	Citric acid	[17]
$Co_{1-x}Zn_xFe_2O_4$ Co-precipitation	Cubic	12—8		fcc spinel structure	Ferrimagnetic	54.1–39.6	9–223	–	10–11	Oleic acid	[18]
$Co_{1-x}Zn_xFe_2O_4$ Solgel	Cubic	13–78	8.39–8.46	–	–	9.81–39.82	95.20- 490.45	400 and 800	9	–	[19]
$Co_xZn_{1-x}Fe_2O_4$ Co-precipitation	–	15–19	-	Single phase	Superparamagnetism	–	–	800	–	–	[36]
$Co_{1-x}Zn_xFe_2O_4$ hydrothermal	Cubic								11	–	[37]
$Co_{0.5}Zn_{0.5}Fe_2O_4$ co-precipitation	Cubic	24–41	8.17–8.41		Superparamagnetism	19.32–66.58	96–135	500–1000	11–11.5		[20]
$Zn_xCo_{1-x}Fe_2O_4$ microwave combustion	Cubic	25–29	8.43–8.44	Mixed spinel	Ferromagnetic;super paramagnetism	2.09–64.85	–	–	–	–	[38]
$Co_{1-x}Zn_xFe_2O_4$ combustion	Cubic	6–13	8.38–8.43	Single-phase ferrite	Superparamagnetism	–	–	–	–	–	[39]
$Co_{1-x}Zn_xFe_2O_4$ co-precipitation	Cubic	–	8.55–8.61	–	–	52.39–89.84	9–159	1000–1100	11	–	[15]

Table 3 (continued)

Compound and method	Structure	*D* (nm)	*a* (Å)	FST	MST	M_S emu/g	Hc Oe	C_T (°C)	S	R
$Co_{0.5}Zn_{0.5}Fe_2O_4$ ball milling	Cubic	–		–	Ferromagnetic	1250G	16	1250	–	–	[28]
$Co_{1-x}Zn_xFe_2O_4$ microwave hydrothermal	Cubic	–	–	–	Superparamagnetism	26.04–79.04	–	900	13	–	[21]

D crystallite size; *a* lattice constant; M_s magnetization; H_c coercivity; C_T calcinations temperature; *pH* potential hydrogen; *S* surfactant; *R* reference; *FST* ferrite structure; *MST* magnetic structure

technique. There is a simple description of the single step, cubic spinel structure and space group Fd3m. With addition of zinc in cobalt ferrite, the lattice constant rises from 8.383 to 8.430 Å. As a function of the concentration of zinc, the size of the crystallite ranges from 49 to 45 nm. The magnetization of saturation (M_s = 65.628–5.316 emu/g) demonstrates behavior based on scale. At the octahedral site, the presence of non-magnetic (Zn^{2+}) in the cobalt ferrite spinel lattice introduces spin canting, which reduces magnetization (M_s). Anisotropy continuously decreases with increased Zn^{2+} content, and the coercive force magnitude decreases. With increasing Zn^{2+} in cobalt ferrite, the explanation for decreasing coercivity (1116.9→113.48 Oe) is the decrease in magneto-crystalline anisotropy by migrating Co^{2+} ions to the tetrahedral (A) site and decreasing the concentration of Fe^{2+} ions at the octahedral sites in the spinel lattice because Fe^{2+} ions are also the source of magnetic anisotropy in ferrites [14]. $Co_{0.50}Zn_{0.50}Fe_2O_4$ was synthesized by an adapted sol–gel process [33]. Co-doped $ZnFe_2O_4$ exhibits the structure of the cubic spinel. No further reflections were detected due to secondary stages.$Co_{0.50}Zn_{0.50}Fe_2O_4$ has an average crystallite size of 13 nm. To synthesize mixed ferrites such as $Co_{1-x}Zn_xFe_2O_4$, the starch-assisted sol–gel auto-combustion process was used [23]. The ferrite's average crystallite size is 22 nm. A single-phase cubic spinel structure is available in the synthesized spinel ferrite nanoparticles. With the Zn substitution in the lattice, it is found that the lattice constant increases. Thus, the lattice constant also increases with the replacement of Zn ions. "Normally, when saturation magnetization (Ms) decreases along with crystallite size, the decrease in Ms is due to the surface effect, also called the dead surface". The dead surface is related to surface spin disorder. As the crystallite size decreases, the number of surface spins in sample increases, so it is predicted that M_S will decrease. Zinc-substituted nanoparticles of cobalt ferrite $Co_{1-x}Zn_xFe_2O_4$ were incorporated using the sol–gel approach [12]. Particle sizes between 11 and 28 nm have been obtained for the prepared ferrites. The lattice parameter values change with zinc concentration (8.477–8.521 Å); this behavior may be due to the replacement of Co^{2+}cation (0.75 Å) with a larger cation Zn^{2+} (0.82 Å) (Table 1). The coercivity value shows a substantial decrease with a rise in zinc substitution from 2000 to 170 Oe. This difference can be due to the decrease in domain wall energy caused by zinc poor magneto-crystalline anisotropy. The replacement of preferential A-site occupancy for non-magnetic cations (Zn^{2+}) results in a decrease in interaction between A- and B-sites in the trade. Therefore, by zinc substitution, the magnetic parameters of ferrite fine particles may be changed. The cobalt-doped zinc ferrite synthesised induced visible-light and the result supports the mixed spinel ferrimagnetisms [11]. Incremental Co^{2+} ion incorporation results in a detectable decrease in the lattice parameter a from 0.8420

to 0.8341 nm, the disparity in the ionic radii of Co^{2+} (0.072 nm) and Zn2 + may be due to that (0.074 nm). However, the $Zn_{0.6}Co_{0.4}Fe_2O_4$ study, presumably due to its higher crystallinity, offers a larger domain size of around 27 nm. The calculated values of magnetization increased gradually from 4 to 6, 8, and 14 emu/g with increasing Co content. As for $Zn_{1-x}Co_xFe_2O_4$ ($x = 0$, 0.03, 0.1, 0.2) samples, their magnetic activity can be explained under the consideration of single-domain nanoparticles because of their small particle size. Since their order temperature is lower than room temperature, at room temperature, the super-exchange interaction between A- and B-site does not appear to be favorable, so they exhibit paramagnetic activity. The $Zn_{0.6}Co_{0.4}Fe_2O_4$ study, however, shows room temperature ferrimagnetisms (Table 2) with observable coercivity of approximately 32Oe and magnetization saturation of ~ 51 emu/g. Preparation of $Co_{1-x}Zn_xFe_2O_4$ samples ($x = 0$, 0.1, 0.2, 0.3, 0.4, 0.5) by co-precipitation process [34]. With a Zn^{2+} doping material, the lattice parameter increases slightly. On the basis of the disparity in ionic radii of Zn^{2+} and Co^{2+}, the growth of a with x can be clarified. The smaller ionic radius of Co (0.58 Å) was replaced by the larger ionic radius of Zn (0.60 Å) due to the expansion of the unit cell, thereby increasing the lattice parameter.

Magnetic measurements display a ferromagnetic behavior, while with the concentration of Zn, the hysteresis loop appears to decrease. At lower amounts, non-magnetic (Zn) ions differentially occupy tetrahedral A-sites, while Zn ions tend to migrate at higher amounts (Fe) to octahedral B-sites of $CoFe_2O_4$. M_s is found to be sensitive to Zn concentration. It is surprisingly interesting that replacing magnetic Co ($\mu B = 3$) with non-magnetic Zn ($\mu B = 0$) results in a magnetization (M_s) increase of 25 percent (M_s). $Co_{0.6}Zn_{0.4}Fe_2O_4$ nanoparticles were synthesized using a single-step hydrothermal process [10]. These particles are ideal for both magnetic hyperthermia and MRI applications. With negligible coercive energy, the particles demonstrate super paramagnetic conduct. A 55 emu/g and 35 Oe were the saturation magnetization and the coercive power of the coated particles, respectively. Such values are lower than those of cobalt ferrites in bulk. Zinc preference drives iron ions into octahedral positions to occupy tetrahedral lattice positions, resulting in an increase in net magnetization. However, the A–B super-exchange interaction in ferrite is weakened by another rise in zinc ions, leading to spin canting and thus reducing saturation magnetization. The coercivity of non-magnetic such as zinc-doped nanoparticles of cobalt ferrite is reduced in comparison with that of nanoparticles of cobalt ferrite. The decline in magneto-crystalline anisotropy with increasing Zn content could be due to this action. Due to a reduction in the number of strongly anisotropic cobalt ions, zinc ions with zero angular momentum incorporated into the cobalt ferrite decrease coercivity. Zn-substituted cobalt ferrite ($Zn_xCo_{1-x}Fe_2O_4$, $x = 0$–1) magnetic nanoparticles were synthesized in alkaline medium by a hydrothermal co-precipitation process [8]. The space group Fd3m refines the cubic spinel ferrite structures. The deduced average NP size decreases marginally with the rise in the volume of zinc. Zinc occupies the A-site most preferably, while cobalt has a higher preference for the B-site, suggesting that both samples are mixed spinels. At a tetrahedral (A) site, the diamagnetic Zn^{2+} ions replace Fe^{3+} ions and the net magnetic moment is increased. The distribution of cations between A-sites and B-sites predicts a maximum value for magnetization, where the incremental occupation of B-sites begins with Zn ions. The decreased remanent magnetization MR/MS results indicate that there could be a transition from hard crystalline to soft tensile stress surface anisotropy in compliance with the coercivity H_C determinations, as zinc ions are substituted in the synthesis of the NPs by cobalt ions. The auto-combustion method has been used to prepare zinc-doped cobalt ferrite nanoparticles with the simple composition of $Co_{1-x}Zn_xFe_2O_4$ [16]. Co–Zn ferrite crystallizes in the cubic system of spinel form belonging to the space group Fd^3m. The estimated mean size of the crystallite is in the 34–45 nm range. The improvement in the zinc-concentration lattice values of parameter '*a*' (8.37–8.44 Å) is attributed to the fact that the ionic radii of cobalt ions are lower than those of zinc ions. Nanocrystalline $Co_{1-x}Zn_xFe_2O_4$ (0.0–0.1) ferrites were synthesized using a simple, economical and environmentally friendly method of auto-combustion of sucrose [35]. Inside the octahedral sites, $Co_{1-x}Zn_xFe_2O_4$ ferrites displacing Co^{2+} ions occupied and eventually shifting the scheme from opposite to regular spinel. A minor alteration in the peak positions in accordance with this approach would have been needed due to the variations in the ionic radii of the total ions and their favored site occupation. No such obvious change in peak position was carried out in the present method, which revealed the preferential occupation of Zn2 + ions at octahedral sites by replacing Co^{2+} ions of exactly the same ionic radius. The very slight modification in the lattice parameters obtained by gradual Zn-substitution is easily explained by this behavior. Enhancements in magnetization by the incorporation of zinc should be discussed in relation to the influence of cationic stoichiometry and its favored occupancy at various sites. The mechanism of super-exchange interaction between metal ions of the tetrahedral (A-sites) and octahedral (B-sites) can generally be due to the magnetic order in the ferromagnetic cubic spinel. In literature, by increasing Zn content, several authors reported a decreasing magnetization activity in the $Co_{1-x}Zn_xFe_2O_4$ ferrite system. A relatively high magnetization value (67.6 emu/g) was observed compared to other cobalt ferrites prepared using other methods. Usually, the Zn^{2+} ion replacement (with zero magnetic moment and preferring A-site occupancy) results in the super-exchange interaction being

decreased and the magnetic properties are thus varied by changing their concentration. However, in view of the cations distribution suggested through structural studies, the unexpected changes in the magnetization values by adding zinc can be defined in this paper. Microwave gel combustion has successfully synthesised zinc-doped $CoFe_2O_4$ nanoparticles of the formulation $CoFe_{2-x}Zn_xO_4$ [17]. By adding Zn ion to the ($CoFe_2O_4$) CFO matrix, the unmodified spinel structure obtained indicates that the Zn dopant should be incorporated as a replacement ion into the lattice. Increase the CFO lattice parameters from 8.35 to 8.58 nm by increasing the Zn concentration from zero to 15 percent. On the basis of Vegard's law, which can be due to the greater ionic radius of Zn^{2+} (0.74 Å) (Table 1) compared to Fe^{3+} (0.64 Å), this increase in the lattice parameter and volume of the unit cell can be easily explained. The CFO recorded 12.38 nm for pure crystallite, 15 percent for Zn-doped CFO and increased to 15.79 nm. The lattice parameter ranges from 8.351–8.585 Å as Zn increases. The Zn concentration in crystalline size, lattice parameter and density are responsible for these variations. Ultrafine particles of $Co_{1-x}Zn_xFe_2O_4$ with x varying between 0.1 and 0.5 were prepared using the co-precipitation method [18]. The material reveals the presence of the single-phase FCC spinel structure in both investigations. The particle size is decreased from 12 to 8 nm as the partial zinc substitution increases. The order is primarily due to the super-exchange process of interaction between the metal ions in the A and B sublattices in the ferrimagnetic spinel cubic structure. The substitution of non-magnetic ions such as Zn, which have a preferential A-site occupancy, results in a decrease in the interaction between sites A and B. The magnetization of saturation decreased from 54.1 to 39.6 emu/g, while the zinc concentration increased from 0.1 to 0.5. Owing to the size effect or to the presence of super magnetic particles, the decrease in magnetic properties may be due to a partial substitution of non-magnetic zinc. The further increase in zinc substitution also leads to a 0.5 emu/g and 9.8 Oe reductions in remanence and coercivity for $Co_{0.5}Zn_{0.5}Fe_2O_4$, respectively. The saturation magnetization of the fluid samples decreases as the partial substitution of zinc with cobalt grows. Ferrofluids with $Co_{0.5}Zn_{0.5}Fe_2O_4$fine particles (with broad magnetic volume force) can be used effectively for energy conversion applications. $Co_{1-x}Zn_xFe_2O_4$ ($x=0.3$, 0.5, 0.7) and $ZnFe_2O_4$ were prepared [19] using the sol–gel process. The particle size increases from 13 to 19 nm linearly for 400 °C sintered samples as a function of decreasing zinc concentration. With theexception of $x=0.5$, the particle size decreases from 78 to 45 nm for sintered samples of 800 °C, which is due to the difference in ionic radii of Cobalt (Co^{2+} (0.72)) and zinc (Zn^{2+} (0.74)). Sintering temperatures for zinc concentrations $x=0.7$ and 0.5 were found to be an irregular shift in the lattice parameter. This difference is due to nanosized particles that, compared to the bulk material, are associated with a strong cohesive energy. The occupation index of sites A and B is highly dependent on the conditions of synthesis, such as particle size, temperature, and pressure. The transition of $Fe^{2+}\leftrightarrow Fe^{3+}$ or $Co^{2+}\leftrightarrow Co^{3+}$ or $Zn^{2+}\leftrightarrow Zn^{3+}$ ions may be responsible for ferrite conduction due to the hopping of charge carriers between neighbouring octahedral sites (B). In comparison, because of the increased sintering temperature (i.e.) bulk behavior of the samples without any surface contribution entirely controlled by cations distribution, 800 °C sintered samples behave differently. Therefore, as an ionic radius of Fe is (0.67), Zn atoms ideally appear to occupy B-site rather than A-site. When the particle size is very large, the surface contribution reduces and magnetization is just the outcome of the inversion of cations. Spin canting and non-collinear spin arrangement do not lead to a decrease in M_s (due to an increased particle size of 78.59 nm) because Ms does not increase with respect to particle size. The reduction of saturation magnetization can also be explained in terms of its non-collinear spin configuration at or near the atom's surface. Due to the spin canting effect, the decrease in M_s. Zn-doped cobalt ferrite sintered at 800 °C exhibits a semiconducting nature, of all things. Ceramic nanoparticles of $Co_xZn_{1-x}Fe_2O_4$were synthesized by co-precipitation process [36].The variation (Zn) particle sizes and lattice parameters were affected shift of cobalt cations in ferrite system. Compared to the octahedral sites, Zn^{2+} and Fe + ions have a very strong preference for tetrahedral sites in such a framework (spinel structure).

Co^{2+} ions, on the other hand, have a powerful preference for octahedral sites. The introduction of Co^{2+} ions into the system, therefore, induces a rise in iron ion concentration at tetrahedral sites, which is energetically more favorable for Fe^{3+} ions. In addition, the rise in the doping crystallite size up to $x=0.7$ can also be explained by the cobalt's electronic structure ($3d^7$) and its preference to interact with ligands and oxygen anions compared to the ideal electronic structure of Zn^{2+}. The absence of the unpaired electron in Zn^{2+}, s or d orbital contributes to limited covalent interaction and choice between $Zn^{2+}$and their ligands for extension. Therefore, by replacing Co^{2+} ions with Zn^{2+}ions, the strength of the covalent interaction and preference to interact with ligands will be enhanced. As a consequence, an increase in saturation magnetization is seen by increasing Co. In addition, for all the prepared samples at room temperature, superparamagnetic activity and greater surface area were observed, resulting from the state of our powder synthesis. The hydrothermal method was used to prepare nanocrystalline cobalt ferrites substituted with Zn with the formula $Co_{1-x}Zn_xFe_2O_4$ ($x=0.0$–1.0). High physical properties such as high chemical stability, high corrosion resistance, magneto-crystalline anisotropy, magnetostriction and magneto-optical properties have been demonstrated. If the content of the Zn increases,

the lattice constant for each composition increases and follows the law of Vegard. As the ion size of Co^{2+} (0.72 Å) is smaller than that of Zn^{2+} (0.74 Å), this may be due to variations in the ion sizes of Zn^{2+} and Co^{2+} cations. Consequently, the lattice constants were found to be inside the lattice constant range of $ZnFe_2O_4$ and $CoFe_2O_4$ [37]. In this paper, nanoparticles (NPs) of cobalt zinc ferrite ($Co_{0.5}Zn_{0.5}Fe_2O_4$) were prepared using the chemical co-precipitation method [20]. This work deals with the synthesis of $Co_{0.5}Zn_{0.5}Fe_2O_4$ NPs via the process of co-precipitation, their annealing for the study of physical properties at different temperatures characterization. Fig. 6 shows the Variation of magnetic signature due to calcinations temperature with the increase in annealing temperature, enhancement in crystallinity and crystallite size is observed. The morphology and grain size of prepared NPs have also been greatly influenced by annealing. With a raise in the annealing temperature (Fig. 6), the $Co_{0.5}Zn_{0.5}Fe_2O_4$ NPs demonstrated a remarkable change in the magnetic moment. As the samples' annealing temperature increases, the crystallite size increases. The difference between the atomic masses of cobalt and zinc, which influences the NP density due to an increase in the amount of samples prepared at the temperature of the annealing. With the rise in annealing temperature, the porosity of ferrite NPs is found to decrease. The annealing temperature of coercivity (H_c) greatly affects the Hc of prepared nanoferrite. Hc has sinusoidal activity and shows large values for synthesized ferrite NPs ranging from 96.88 to 113.5 Oe. The consequence of crystalline size may be due to this variation in Hc values. Due to surface effects, Hc increases with the rise in crystallite size. And with the rise in crystallite size, H_c continues to decrease above the critical crystallite size. The number of grain boundaries rises by the rise in crystallite size, and thus H_c of NPs decreases. Therefore, with the increased annealing temperature, the decrease

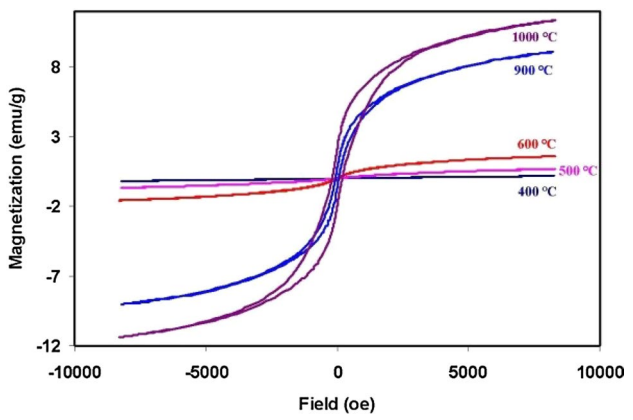

Fig. 6 Variation of magnetic signature due to calcinations temperature (reproduced from Ref. [40] with permission from Chemistry Central Journal)

in H_c can be attributed to a decrease in the anisotropy field that decreases the domain wall energy in response. Using the microwave combustion process, $Zn_xCo_{1-x}Fe_2O_4$ spinel nanoparticles (NPs) were synthesized [38]. This paper discussed that during the microwave combustion process, a well-defined, pure, single-phase spinel structure was formed without any impurity and other phase formation. The centres of the two most extreme peaks (220) and (311) are slightly moved to the lower diffracted angles, with the concentration of Zn^{2+} dopant rising, due to the difference in the ionic radii of the ions Zn^{2+} (0.82 Å) and Co^{2+} (0.72 Å) and the presence of Zn^{2+}dopant in the $CoFe_2O_4$ spinel matrix was also verified. With an increase in Zn^{2+}material, the strength of diffraction peaks decreased significantly, which suggests that the increase in the concentration of Zn^{2+}doping ($x = 0.4$) retards the size of the crystallite. The value of the undoped $CoFe_2O_4$ lattice parameter is $a = 8.432$ Å and the value increases from 8.434 to 8.441 Å with an increase in the Zn^{2+} content ($x = 0.2$ to 1.0). The lattice parameter values show an almost linear dependency, thus obeying the law of Vegard. The magnetic properties of the spinel ferrites typically depend on the composition and distribution of the cations between the occupation of the A- and B- sites, and they may be ferromagnetic, antiferromagnetic, and paramagnetic in nature. Ferromagnetic activity is shown by the undoped $CoFe_2O_4$ sample, and magnetization (M_s) increased (64.85 emu/g) with the applied field and does not saturate even at + 10 kOe. The prepared lower composition ($x = 0.0$, 0.2, and 0.4) shows a ferromagnetic behavior and the higher compositions ($x = 0.6$, 0.8 and 1.0) display a super paramagnetic behavior (with hysteresis, and with rising Zn^{2+} material, the M_s Values decreased. Similarly, the lattice defects, magnetic super-exchange interaction from the A-sites to B-sites, and magnetic super-exchange interaction from A to B- sites are due to the observed M_s values of the samples. However, with the increase in Zn^{2+} material, which can be due to the magnetic character and anisotropic nature of spinel Co–Zn ferrites, It has been found that H_c, M_r and M_s values of the spinel $Zn_xCo_{1-x}Fe_2O_4$ NPs have steadily decreased. Nanoparticle $Co_{1-x}Zn_xFe_2O_4$ samples were prepared using alove vera gel through the route of combustion [39]. Nanoparticle $Co_{1-x}Zn_xFe_2O_4$ samples have been prepared using alove vera gel via the combustion path. It was found that $ZnFe_2O_4$ has a regular spinel structure, whereas $CoFe_2O_4$ has an inverse spinel structure. However the tetrahedral and octahedral positions are often occupied by the $Co_{1-x}Zn_xFe_2O_4$ ferrite nanoparticles with intermediate character of regular spinel structure and inverse spinel structure due to Zn and Co atoms. Zinc-substituted cobalt ferrite, $Co_{1-x}Zn_xFe_2O_4$ Wet chemical co-precipitation accompanied by sintering at 1000 °C was synthesized [15]. It was discovered that the individual sample density diminished with an expansion in the Zn material. The impact on the lattice

constant and grain size of the grouping of zinc. The increment in zinc content was seen at the tetrahedral and octahedral locales in the grid consistent, porosity, ionic radii, distance between the attractive particles and bond lengths. Zincreconciliation is because of the development of iron particles from the tetrahedral site to the octahedral site. Zinc replacement significantly affects underlying and magnetic properties like saturation magnetization, coercivity, temperature of Curie. It is important to recall that the difference in grid constants with Zn content keeps Vegard's law for all examples. There is an improved lattice constant with the ascent in zinc content and sintering temperature. This is probably due to the difference in the surface to volume ratio in the bulk state. The increase of the lattice constant can be explained on the basis of the stoichiometry of the cations at a particular condition of the $Co_{1-x}Zn_xFe_2O_4$ ferrite nanoferrite system. Based on the cations distribution and super-exchange mechanism of interaction between iron (A-sites) and cobalt ions (B-sites) in cubic ferromagnetic spinels, the magnetic order is generally clarified. Non-magnetic ion Zn prefers occupation of A-sites, which in turn leads to a decrease in the exchange interaction between A- and B-sites, resulting in a strengthening of the B–B interaction. Some trivalent iron ions move from A-site to B-site with Zn^{2+} ion substitution according to the site preferences of different ions, raising the Fe^{2+} ions at B-sites. By leaving A-sites, the number of iron ions becomes small with the growth of Zn content, which in turn causes a decrease in A–B interaction encountered at B-sites by iron ions. As the number of Fe^{2+} ions increases at B-sites, an increase in B–B interaction is induced and spin canting occurs as a result. The decrease in coercivity value with increasing Zn^{2+} content may be attributed to the sample's direct link with the anisotropy constant, which arises from crystal imperfection and the high degree of aggregation. With the increase in the content of Zn^{2+}, the domain wall energy is also decreased as the known anisotropy effect of Co decreases. On the basis of domain structure and the anisotropy of the crystal, the shift in coercivity (H_C) value can be clarified. This magnetic ferrite material is a suitable possible candidate for use for storage devices. In this research report, magnetic and microwave absorption loss and other reaction characteristics in composite cobalt zinc ferrite were studied [28]. This composite is used to absorb material from the microwave. The strength of the major peaks belonging to cubic spinel ferrite was increased by sintering at 1250 °C, demonstrating the improvement in the degree of crystallinity of the prepared samples, as well as the strain released during the process of high energy ball milling. The displacement of Co^{2+} at the Zn^{2+} site resulted in the transfer of Fe^{3+} to the A-site and the approach of Co^{2+} to fill the B-site vacancy. The magnetic interaction between the Fe^{3+} on the A-site and the Co^{2+} and Fe^{3+} on the B-site has, therefore, been improved. This study outcome and results were an attempt to solve and improvise the conventional spinel ferrite problem that is used as an effective microwave absorber.

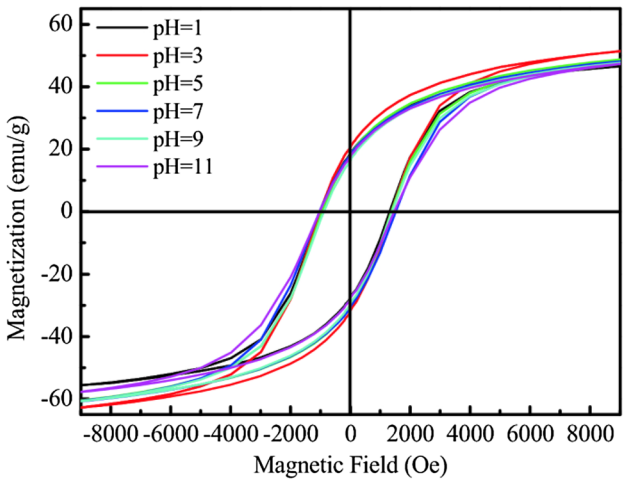

Fig. 7 Variation of magnetic signature due to pH (reproduced from Ref. [41] with permission from Applied Physics A)

Figure 7 shows the variation of magnetic signature due to pH. Nanopowders with the stoichiometric composition $Co_{1-x}Zn_xFe_2O_4$ were prepared using a hydrothermal microwave process [21]. All the samples were synthesized with a pH of ~ 13. The magnetic ions of the tetrahedral A-site are so much reduced when higher Co^{2+}ions are substituted by Zn^{2+}ions in the $Co_{1-x}Zn_xFe_2O_4$, that the dominant inter-sublattice A–B super-exchange interaction becomes weaker. The intra-sublattice B–B super-exchange interaction thus enhances, resulting in the occurrence of spontaneous spin canting on the B-site with regard to the direction of the A-site's spins. It can therefore be reasonably inferred that canted (non-collinear) spins contribute to a decrease in Zn concentration values of the magnetic moment (and magnetization). The concentration of the Co^{2+}ions at the octahedral (B) sites decreases as the Zn concentration increases in cobalt ferrite, leading to a decrease in effective magnetic anisotropy. In terms of the cation distribution and grain size effect, the magnetic properties are explained. Thus, the high permeability, moderate M_s and H_c displayed by the Zn-doped nanocrystals $CoFe_2O_4$ are favorable for their possible use as a ferrite head in high-density recording media applications.

Conclusion

The structural and magnetic characteristics of ferrites are present in this review paper. Co–Zn ferrite integrated and its cubic structure phase at 400 °C to 1250 °C. So, temperature is a major role in controlling ferrite crystallinity, phase purity, structural and magnetic properties. The average

particle size find from 9 to 90 nm. The lattice constant varied from 8.33 to 8.61 Å. The crystallite size and lattice constant was influenced as it mixed cobalt ferrite into zinc. Magnetic specifications such as magnetization and coercivity changed from 0.31 to 79.04 emu/g and 9 Oe to 1265 Oe, respectively, when dopant (Zn^{2+}) increased. These employed mixed ferrites exhibits superparamagnetism signature after calcinations. As surfactants (PVP/PVA/Citric acid) are strongly controlled nanosized and magnetic properties. The pH value (7–13) is most significance for affecting the adsorption behavior; modify surface charge and migration cations as well. Co–Zn mixed ferrite are used in various industrial and medical field such as optical recording media, magnetic sensors, magnetic hyperthermia, storage device, microwave absorbing materials, waste water treatment and MRI.

Acknowledgements One of the authors is R. Sagayaraj, thank Rev. Fr. G. Peter Rajendiram., Secretary, St. Joseph's College of Arts & Science, Cuddalore, India, for their continuous encouragement. And also thank Rev. Fr. Dr. S. Xavier, Department of Physics, St. Joseph's College of Arts & Science, Cuddalore, India, for their constant support.

Declarations

Conflict of interest The authors declare that they have no known competing financial interests or personal relationships that could have appeared to influence the work reported in this paper.

References

1. Sagayaraj, R., Aravazhi, S., Praveen, P., Chandrasekaran, G.: Structural, morphological and magnetic characters of PVP coated $ZnFe_2O_4$ nanoparticles. J. Mater. Sci. **29**(3), 2151–2158 (2017). https://doi.org/10.1007/s10854-017-8127-4
2. Sagayaraj, R., Aravazhi, S., Chandrasekaran, G.: Effect of zinc content on structural, functional, morphological, resonance, thermal and magnetic properties of $Co_{1-x}Zn_xFe_2O_4$/PVP nanocomposites. J. Inorg. Organomet. Polym. Mater. **29**, 2252–2261 (2019). https://doi.org/10.1007/s10904-019-01183-3
3. Sagayaraj, R., Aravazhi, S., Selvakumar, C., Senthilkumar, S., Chandrasekaran, G.: Tuning of ferrites ($Co_xFe_{3-x}O_4$) nanoparticles by co-precipitation technique. SN Appl. Sci. **1**(3), 271 (2019). https://doi.org/10.1007/s42452-019-0244-7
4. Sagayaraj, R., Aravazhi, S., Chandrasekaran, G.: Synthesis, spectroscopy, and magnetic characterizations of PVP-assisted nanoscale particle. J. Supercond. Nov. Magn. **31**, 3379–3386 (2018). https://doi.org/10.1007/s10948-018-4593-z
5. Sagayaraj, R., Dhineshkumar, T., Prakash, A., Aravazhi, S., Chandrasekaran, G., Jayarajan, D., Sebastian, S.: Fabrication, microstructure, morphological and magnetic properties of w-type ferrite by co-precipitation method: Antibacterial activity. Chem. Phys. Lett. **759**, 137944 (2020). https://doi.org/10.1016/j.cplett.2020.137944
6. Kaur, A., Bhargava, G.K.: Review paper on nickel-zinc nano ferrite. Mater. Today (2020). https://doi.org/10.1016/j.matpr.2020.09.016
7. Vijayaprasath, G., Murugan, R., Hayakawa, Y., Ravi, G.: Optical and magnetic studies on Gd doped ZnO nanoparticles synthesized by co-precipitation method. J. Lumin. **178**, 375–383 (2016). https://doi.org/10.1016/j.jlumin.2016.06.004
8. Coppola, P., da Silva, F.G., Gomide, G., Paula, F.L.O., Campos, A.F.C., Perzynski, R., Aquino, R.: Hydrothermal synthesis of mixed zinc–cobalt ferrite nanoparticles: structural and magnetic properties. J. Nanopart. Res. (2016). https://doi.org/10.1007/s11051-016-3430-1
9. Hian, H., et al.: Localized manipulation of magnetic particles in an ensemble. IEEE Access **6**, 24075–24088 (2018). https://doi.org/10.1109/ACCESS.2018.2829715
10. Ahmad, A., Bae, H., Kim, C., Rhee, I.: Characterization of zinc-doped cobalt ferrite nanoparticles for application as heat generators in magnetic hyperthermia and MRI contrast agents. J. Korean Phys. Soc. **74**(12), 1151–1159 (2019). https://doi.org/10.3938/jkps.74.1151
11. Fan, G., Tong, J., Li, F.: Visible-light-induced photocatalyst based on cobalt-doped zinc ferrite nanocrystals. Ind. Eng. Chem. Res. **51**(42), 13639–13647 (2012). https://doi.org/10.1021/ie201933g
12. Ben Ali, M., El Maalam, K., El Moussaoui, H., Mounkachi, O., Hamedoun, M., Masrour, R., Benyoussef, A.: Effect of zinc concentration on the structural and magnetic properties of mixed Co–Zn ferrites nanoparticles synthesized by sol/gel method. J. Magn. Magn. Mater. **398**, 20–25 (2016). https://doi.org/10.1016/j.jmmm.2015.08.097
13. Tapeinos, C.: Magnetic Nanoparticles and Their Bioapplications, Smart Nanoparticles for Biomedicine, pp. 131–142. Elsevier, Amsterdam (2018)
14. Raut, A.V., Barkule, R.S., Shengule, D.R., Jadhav, K.M.: Synthesis, structural investigation and magnetic properties of Zn^{2+} substituted cobalt ferrite nanoparticles prepared by the sol–gel auto-combustion technique. J. Magn. Magn. Mater. **358–359**, 87–92 (2014). https://doi.org/10.1016/j.jmmm.2014.01.039
15. Nasrin, S., Chowdhury, F.-U.-Z., Hasan, M.M., Hossen, M.M., Ullah, S.M., Hoque, S.M.: Effect of zinc substitution on structural, morphological and magnetic properties of cobalt nanocrystalline ferrites prepared by co-precipitation method. J. Mater. Sci. **29**, 18878–18889 (2018). https://doi.org/10.1007/s10854-018-0013-1
16. Nayeem, F., Parveez, A., Chaudhuri, A., Sinha, R.R., Khader, S.A.: Effect of Zn^{+2} doping on structural, dielectric and electrical properties of cobalt ferrite prepared by auto combustion method. Mater. Today **4**(11), 12138–12143 (2017). https://doi.org/10.1016/j.matpr.2017.09.142
17. Agrawal, S., Parveen, A., Azam, A.: Structural, electrical, and optomagnetic tweaking of Zn doped $CoFe_{2-x}Zn_xO_{4-\delta}$ nanoparticles. J. Magn. Magn. Mater. **414**, 144–152 (2016). https://doi.org/10.1016/j.jmmm.2016.04.059
18. Arulmurugan, R., Vaidyanathan, G., Sendhilnathan, S., Jeyadevan, B.: Co–Zn ferrite nanoparticles for ferrofluid preparation: Study on magnetic properties. Phys. B Condens. Matter **363**(1–4), 225–231 (2005). https://doi.org/10.1016/j.physb.2005.03.025
19. Arunkumar, A., Vanidha, D., Kannan, R., Shanmugam, M.: Unusual transition of electrical and magnetic properties in the nano to bulk transformation of Co–Zn ferrites. J. Supercond. Nov. Magn. **33**, 2109–2123 (2020). https://doi.org/10.1007/s10948-020-05448-8
20. Iqbal, J., Rajpoot, M., Jan, T., Ahmad, I.: Annealing Induced enhancement in magnetic properties of $Co_{0.5}Zn_{0.5}Fe_2O_4$ nanoparticles. J. Supercond. Nov. Magn. **27**(7), 1743–1749 (2014). https://doi.org/10.1007/s10948-014-2505-4
21. Praveena, K., Sadhana, K., Liu, H.-L., Murthy, S.R.: Effect of Zn substitution on structural, dielectric and magnetic properties of nanocrystalline $Co_{1-x}Zn_xFe_2O_4$ for potential high density recording media. J. Mater. Sci. **27**(12), 12680–12690 (2016). https://doi.org/10.1007/s10854-016-5402-8
22. Dhir, G., Uniyal, P., Verma, N.K.: Effect of particle size on multiferroism of barium-doped bismuth ferrite nanoparticles. Mater.

Sci. Semicond. Process. **27**, 611–618 (2014). https://doi.org/10.1016/j.mssp.2014.07.041
23. Yadav, R.S., Havlica, J., Hnatko, M., Šajgalík, P., Alexander, C., Palou, M., Enev, V.: Magnetic properties of $Co_{1-x}Zn_xFe_2O_4$ spinel ferrite nanoparticles synthesized by starch-assisted sol–gel auto-combustion method and its ball milling. J. Magn. Magn. Mater. **378**, 190–199 (2015). https://doi.org/10.1016/j.jmmm.2014.11.027
24. Mohapatra, J., Liu, J.P.: Rare-earth-free permanent magnets: The past and future. Handb. Magn. Mater. **27**, 1–57 (2018)
25. Sahoo, B., Devi, K.S.P., Dutta, S., Maiti, T.K., Pramanik, P., Dhara, D.: Biocompatible mesoporous silica-coated superparamagnetic manganese ferrite nanoparticles for targeted drug delivery and MR imaging applications. J. Colloid Interface Sci. **431**, 31–41 (2014). https://doi.org/10.1016/j.jcis.2014.06.003
26. Khanna, L., Verma, N.K.: Size-dependent magnetic properties of calcium ferrite nanoparticles. J. Magn. Magn. Mater. **336**, 1–7 (2013). https://doi.org/10.1016/j.jmmm.2013.02.016
27. Nogueira, N.A.S., Utuni, V.H.S., Silva, Y.C., Kiyohara, P.K., Vasconcelos, I.F., Miranda, M.A.R., Sasaki, J.M.: X-ray diffraction and Mossbauer studies on superparamagnetic nickel ferrite ($NiFe_2O_4$) obtained by the proteic sol–gel method. Mater. Chem. Phys. **163**, 402–406 (2015). https://doi.org/10.1016/j.matchemphys.2015.07.057
28. Hapishah, A.N., Syazwan, M.M., Hamidon, M.N.: Synthesis and characterization of magnetic and microwave absorbing properties in polycrystalline cobalt zinc ferrite ($Co_{0.5}Zn_{0.5}Fe_2O_4$) composite. J. Mater. Sci. **29**, 20573–20579 (2018). https://doi.org/10.1007/s10854-018-0192-9
29. Ghasemi, A., Ekhlasi, S., Mousavinia, M.: Effect of Cr and Al substitution cations on the structural and magnetic properties of $Ni_{0.6}Zn_{0.4}Fe_{2-x}Cr_{x/2}Al_{x/2}O_4$ nanoparticles synthesized using the sol–gel auto-combustion method. J. Magn. Magn. Mater. **354**, 136–145 (2014). https://doi.org/10.1016/j.jmmm.2013.10.022
30. Slimani, Y., Algarou, N.A., Almessiere, M.A., Sadaqat, A., Vakhitov, M.G., Klygach, D.S., Tishkevich, D.I., Trukhanov, A.V., Güner, S., Hakeem, A.S., Auwal, I.A., Baykal, A., Manikandan, A., Ercan, I.: Fabrication of exchange coupled hard/soft magnetic nanocomposites: Correlation between composition, magnetic, optical and microwave properties. Arab. J. Chem. **14**(3), 102992 (2021)
31. Durmus, Z., Kavas, H., Durmus, A., Aktaş, B.: Synthesis and micro-structural characterization of graphene/strontium hexaferrite ($SrFe_{12}O_{19}$) nanocomposites. Mater. Chem. Phys. **163**, 439–445 (2015). https://doi.org/10.1016/j.matchemphys.2015.07.063
32. Thakur, A., Singh, R.R., Barman, P.B.: Synthesis and characterizations of Nd^{3+} doped $SrFe_{12}O_{19}$ nanoparticles. Mater. Chem. Phys. **141**(1), 562–569 (2013). https://doi.org/10.1016/j.matchemphys.2013.05.063
33. Lima-Tenório, M.K., Tenório-Neto, E.T., Garcia, F.P., Nakamura, C.V., Guilherme, M.R., Muniz, E.C., Rubira, A.F.: Hydrogel nanocomposite based on starch and Co-doped zinc ferrite nanoparticles that shows magnetic field-responsive drug release changes. J. Mol. Liq. **210**, 100–105 (2015). https://doi.org/10.1016/j.molliq.2014.11.027
34. Tatarchuk, T., Bououdina, M., Macyk, W., Shyichuk, O., Paliychuk, N., Yaremiy, I., Pacia, M.: Structural, optical, and magnetic properties of Zn-doped $CoFe_2O_4$ nanoparticles. Nanoscale Res. Lett. (2017). https://doi.org/10.1186/s11671-017-1899-x
35. Gabal, M.A., Al-Juaid, A.A., Al-Rashed, S.M., Hussein, M.A., Al-Marzouki, F.: Synthesis, characterization and electromagnetic properties of Zn-substituted $CoFe_2O_4$ via sucrose assisted combustion route. J. Magn. Magn. Mater. **426**, 670–679 (2017). https://doi.org/10.1016/j.jmmm.2016.10.147
36. Mehran, E., FarjamiShayesteh, S., Nasehnia, F.: Investigation of structural and magnetic effects of cobalt doping in $ZnFe_2O_4$ nanoparticles. J. Supercond. Nov. Magn. **29**(5), 1241–1247 (2016). https://doi.org/10.1007/s10948-016-3415-4
37. Ünal, B., Baykal, A.: Effect of Zn substitution on electrical properties of nanocrystalline cobalt ferrite. J. Supercond. Nov. Magn. **27**(2), 469–479 (2013). https://doi.org/10.1007/s10948-013-2285-2
38. Hema, E., Manikandan, A., Karthika, P., Antony, S.A., Venkatraman, B.R.: A novel synthesis of Zn^{2+}-doped $CoFe_2O_4$ spinel nanoparticles: Structural, morphological, opto-magnetic and catalytic properties. J. Supercond. Nov. Magn. **28**(8), 2539–2552 (2015). https://doi.org/10.1007/s10948-015-3054-1
39. Kothawale, M.M., Pednekar, R., Gawas, U.B., Meena, S.S., Prasad, N., Kumar, S.: Characterization of nano-particle $Co_{1-x}Zn_xFe_2O_4$ synthesized using alove vera gel. J. Supercond. Nov. Magn. **30**(2), 395–399 (2016). https://doi.org/10.1007/s10948-016-3745-2
40. Gharagozlou, M.: Influence of calcination temperature on structural and magnetic properties of nanocomposites formed by Co-ferrite dispersed in sol-gel silica matrix using tetrakis(2-hydroxyethyl) orthosilicate as precursor. Chem. Cent. J. **5**(1), 19 (2011)
41. Yu, L., Sun, A., Suo, N., Zuo, Z., Zhao, X., Zhang, W.: Effect of pH on the magnetic properties and microstructure of $Mg_{0.1}Co_{0.9}Fe_2O_4$ prepared by sol–gel self-propagating method. Appl. Phys. A **126**, 615 (2020)